Core-functionalized dendritic oligothiophenes—novel donor–acceptor systems†

Markus K. R. Fischer,[a] Chang-Qi Ma,[a] René A. J. Janssen,[b] Tony Debaerdemaeker[c] and Peter Bäuerle*[a]

Received 2nd March 2009, Accepted 21st April 2009
First published as an Advance Article on the web 26th May 2009
DOI: 10.1039/b904243a

Novel core-functionalized dendritic oligothiophenes (DOT) bearing pyridine or methylpyridinium acceptors have been synthesized up to the third generation. A bathochromic shift in the absorption of the functionalized dendritic oligothiophenes and the appearance of new absorption bands were noticed issuing from an intramolecular charge transfer process. These novel donor–acceptor systems are, due to their broad absorption, promising materials for optoelectronic applications such as organic solar cells. By electrochemical measurements HOMO/LUMO energy levels have been determined and two compounds could be identified with almost ideal energy levels for application in bulk heterojunction solar cells (BHJSC) with fullerene $PC_{61}BM$ as acceptor.

1 Introduction

Three-dimensional branched architectures, generally termed as dendrimers, represent a class of synthetic macromolecules that have had a dramatic impact on the field of organic and polymer chemistry and created a new branch in synthetic and material chemistry. A variety of conjugated dendrimers consisting of conjugated repeating units has been constructed to date with different core, periphery and branching units including the attachment of different functionalities. Their unique properties, such as 3D nanostructures and a monodisperse, defined molecular structure, make them promising materials for electronic applications. Conjugated, rigid and shape-persistent dendritic structures were constructed comprising phenyleneethynylene,[1,2] phenylenevinylene[3] or exclusively phenylene units.[2–4] However, functionalization of dendrimers with oligothiophenes at the core[5–7] or periphery[8–10] as well as only thiophene-based dendrimers[11–13] were also discovered. Dendrimers with different shapes, *e.g.* star-shaped[8,14–20] or tetrahedral,[21–23] have been synthesized. Recently, we introduced novel dendritic oligothiophenes (DOT) up to a 90-mer as a new class of highly soluble 3D macromolecular semiconductors.[24] The synthetic strategy allowed further functionalization at the periphery and/or the core of the conjugated dendrimers as schematically depicted in Fig. 1. Initial applications in organic photovoltaic devices showed good performance (efficiencies up to 1.7% in bulk heterojunction solar cells, BHJSC) and the potential of these structurally defined and solution-processable 3D macromolecular semiconductors.[25]

We already dendronized perylenebisimides as a core with DOTs resulting in oligothiophene-perylene bisimide hybrids with interesting electrochemical and optical properties.[26] This strategy has now been progressed within this work by the introduction of other electron accepting groups, namely pyridine and methylpyridinium units, at the core position of DOTs. Functionalization of oligothiophenes with electron accepting units is a common method to fine tune the electronic properties of materials and hence it is possible to broaden the absorption range and to shift HOMO/LUMO levels to appropriate values.

Pyridine end-capped oligothiophenes were already described in the literature up to a pentamer and synthetic strategies for their synthesis have been investigated, but neither optical nor electrochemical properties have been determined.[27] Thienyls end-capped with pyridine have been found to be good fluorophores[28] and were used in supramolecular chemistry as building blocks for the construction of platina macrocycles.[29] Combination of pyridine with oligothiophenes can be found in donor–acceptor conjugated polymers which showed good electron transport properties and facile charge injection into the polymer due to the electron-withdrawing pyridinyl units.[30] Bipyridine can be found in combination with oligothiophenes in π-conjugated polymers as ligand for complexation of Ru^{II} or Os^{II} which were intensively studied with respect to optical and electronic properties.[31–33] Literature about pyridinium moieties in oligothiophenes can be found only sporadically. Pyridinium functionalities have been introduced into poly(3-hexylthiophene) in order to tune the electronic band structure[34] and have been implemented in nonlinear optical materials[35] and other solvatochromic chromophores due to their strong acceptor ability.[36] Thus, functionalization of oligothiophenes with pyridines or methylpyridinium units resulted in tailored materials with appealing optical and electronic properties. In addition, interesting building blocks for complexation of different metals could be derived.

The aim of this work was to prepare acceptor-functionalized DOTs by systematic variation of the dendrimer generation and the strength of the acceptor group. Novel systems **4**, **5**, **7**, **8**, **10** and **11** represent covalently linked donor–acceptor systems

[a]*Institute of Organic Chemistry II and Advanced Materials, University of Ulm, Albert-Einstein-Allee 11, D-89081 Ulm, Germany. E-mail: peter.baeuerle@uni-ulm.de; Fax: (+49) 731-502-2840*
[b]*Molecular Materials and Nanosystems, Eindhoven University of Technology, P.O. Box 513, NL-5600 MB Eindhoven, Netherlands*
[c]*Institute of Inorganic Chemistry I, University of Ulm, Albert-Einstein-Allee 11, D-89081 Ulm, Germany*

† Electronic supplementary information (ESI) available: Details of the solar cell device fabrication, the analytics and used chemicals; crystal data for **12**. See DOI: 10.1039/b904243a

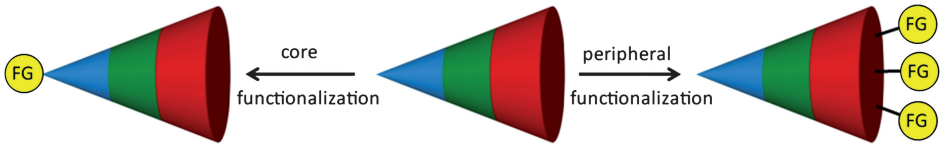

Fig. 1 Core and peripheral functionalization of dendritic oligothiophenes; the cone with its coloured rings represents DOTs of different generations; FG = functional group.

and are compared to the original non-functionalized DOTs which had absorption maxima around 400 nm or less. An extension of the absorption range and a fine-tuning of the frontier orbitals for applications in solution-processable bulk heterojunction solar cells (BHJSC) is expected.

2 Results and discussion

Synthesis

Pyridine-functionalized dendritic oligothiophenes (Py-*n*T: **4** (n = 3), **7** (n = 9), **10** (n = 21)) and their methylated pyridinium derivatives (MePy$^+$-*n*T: **5** (n = 3), **8** (n = 9), **11** (n = 21)) were synthesized up to the third generation (Schemes 1–3). Synthesis of the functionalized DOTs was based on a synthetic route that has already been published by our group.[24] Pyridine was introduced to the core position of the first generation (*G1*) dendritic oligothiophene by Pd-catalyzed Suzuki cross-coupling of 4-iodopyridine and TMS-protected terthienyl boronic acid ester B-3T-Si **1**[37] in 97% yield (Scheme 1). The TMS-protecting groups of Py-3T-Si **2** were removed by trifluoroacetic acid to give pyridine-functionalized *G1*-DOT, Py-3T **4**, in almost quantitative yield. Compound **4** was then reacted with methyl trifluoromethane sulfonate (MeOTf) to give the corresponding methylated pyridinium triflate salt **5** (MePy$^+$-3T) in 93% yield.

The key intermediate for the synthesis of higher generational dendrons is represented by iodinated pyridine functionalized terthiophene Py-3T-I **3**, which was synthesized in 95% yield from **2** by ipso-substitution of the peripheral TMS groups with iodine monochloride. *G2*-pyridine-functionalized dendron Py-9T **7** was then synthesized by Suzuki cross-coupling of **3** with two equivalents of boronic ester B-3T-Si **1** and subsequent deprotection of the TMS groups with tetrabutylammonium fluoride (TBAF) in 90% and 99% yield, respectively (Scheme 2). Methylation to pyridinium salt MePy$^+$-9T **8** was performed with MeOTf in 95% yield.

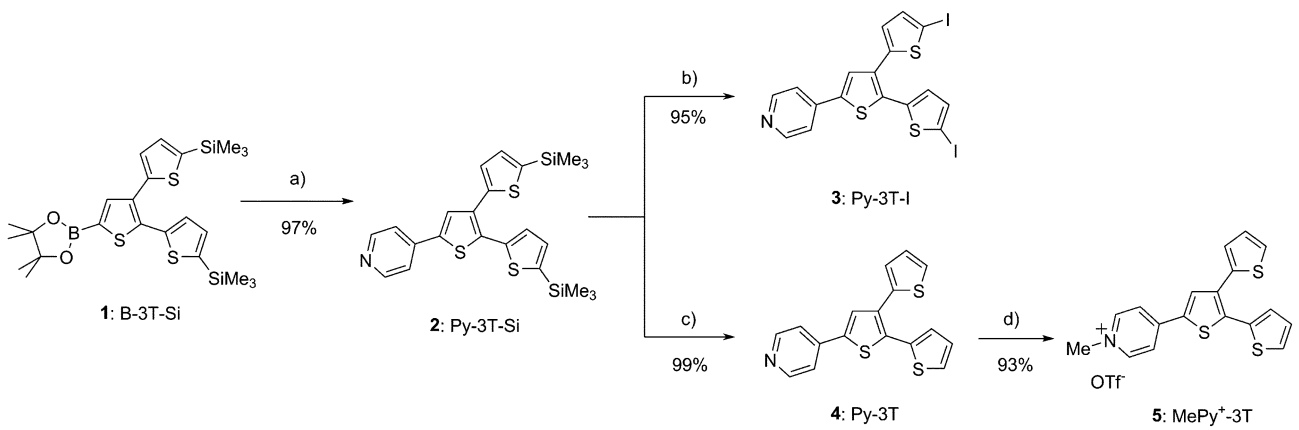

Scheme 1 Synthesis of Py-3T **4** and MePy$^+$-3T **5**. a) 4-Iodopyridine, $[Pd_2(dba)_3]\cdot CHCl_3$, $HP(tBu)_3BF_4$, K_3PO_4; b) ICl; c) CF_3COOH; d) MeOTf, DCM.

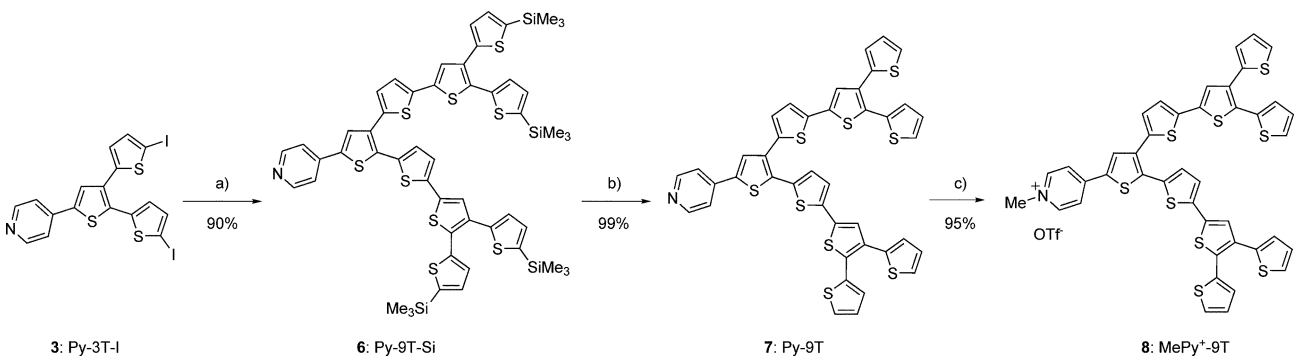

Scheme 2 Synthesis of Py-9T **7** and MePy$^+$-9T **8**. a) B-3T-Si **1**, $[Pd_2(dba)_3]\cdot CHCl_3$, $HP(tBu)_3BF_4$, K_3PO_4; b) TBAF; c) MeOTf, DCM.

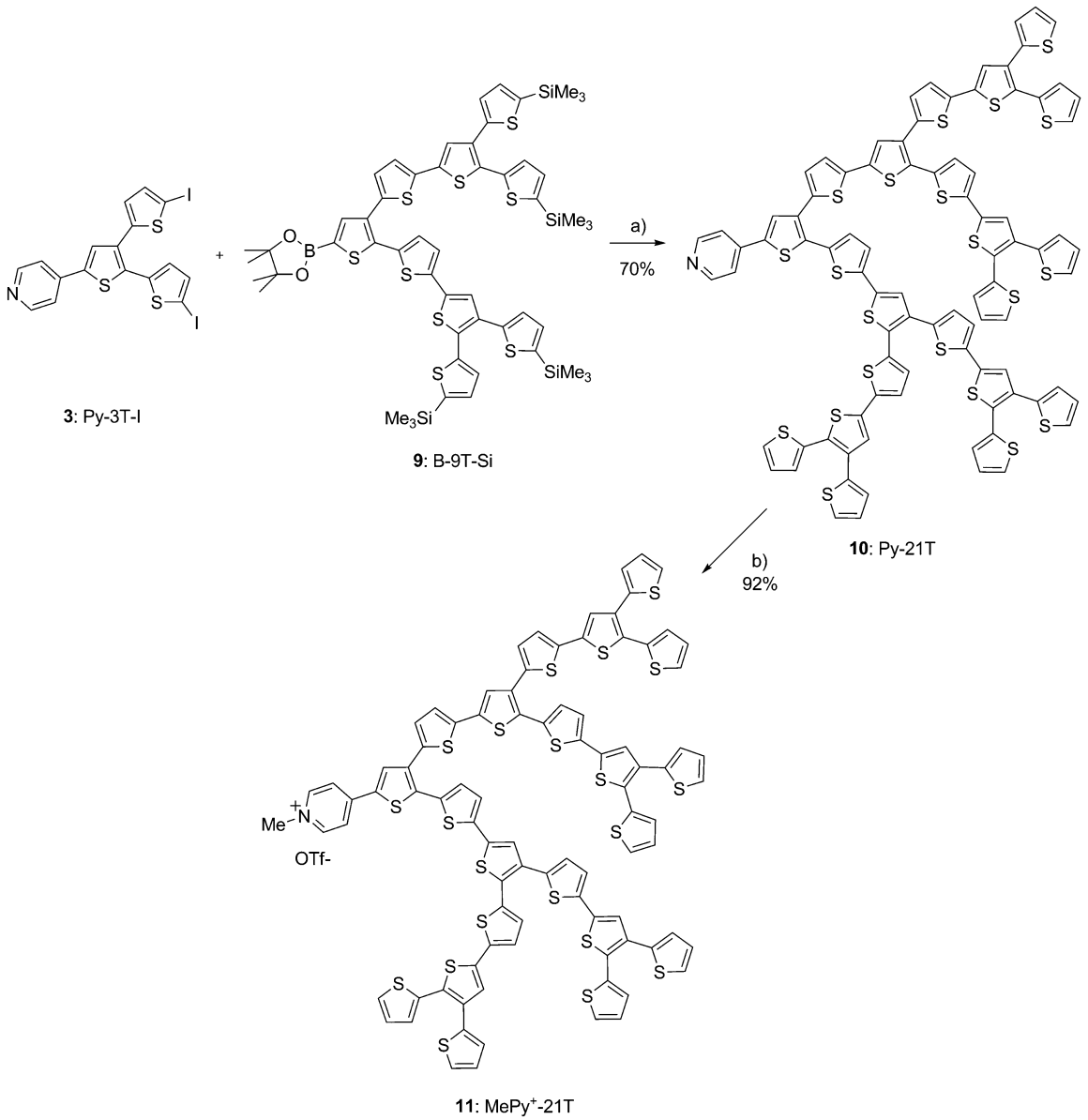

Scheme 3 Synthesis of Py-21T **10** and MePy$^+$-21T **11**. a) 1. $[Pd_2(dba)_3]\cdot CHCl_3$, $HP(tBu)_3BF_4$, K_3PO_4, 2. TBAF; b) MeOTf, 1,4-dioxane.

Similarly, pyridine-functionalized DOT **10** of the third generation was built up in an overall yield of 70% by Suzuki cross-coupling of iodide Py-3T-I **3** with 2 equivalents of second generation boronic ester B-9T-Si **9**[25] and subsequent deprotection with TBAF (Scheme 3). Methylation of **10** to *G3*-pyridinium salt **11** was performed with MeOTf in 1,4-dioxane in 92% yield.

In addition to alkylation, pyridines offer the possibility of metal complexation by a large variety of metal cations. In this respect, and very exemplary, *G1*- and *G2*-pyridine-functionalized DOTs **4** and **7** were reacted with silver(I) triflate, which is known to form linear two-fold coordinated complexes with pyridines.[38] Therefore, a solution of silver triflate in acetonitrile was added to a THF solution of the corresponding DOT ligand and novel DOT-Ag(I) complexes **12** and **13** were prepared in 97% and 92% yield, respectively (Chart 1).

Complexation of silver cations by pyridyl ligands was suggested by ^{1}H NMR spectra, in which two of the pyridyl proton signals were up- and the other two down-field shifted compared to those of the uncomplexed free ligands **4** and **7**. Unequivocal proof of the geometric structure of complex $Ag(Py\text{-}3T)_2{}^+OTf^-$ **12** came from X-ray structure analysis. By recrystallization from acetonitrile suitable single crystals of **12** were obtained. Crystals selected for X-ray analysis were typical of the bulk and there was no indication of polymorphism. Crystallographic data and refinement parameters are given in the ESI.† The coordination surrounding of the silver atom is nearly linear with an angle of 176.7°. The distance between nitrogen and silver atoms was 2.13 Å, comparable to similar complexes comprising a trifluoromethane sulfonate anion (Fig. 2).[39] The pyridine rings (rings A and A′) are coplanar, together with the coordinating silver ion (Fig. 2; rings in parallel planes labelled in blue). Four complexes

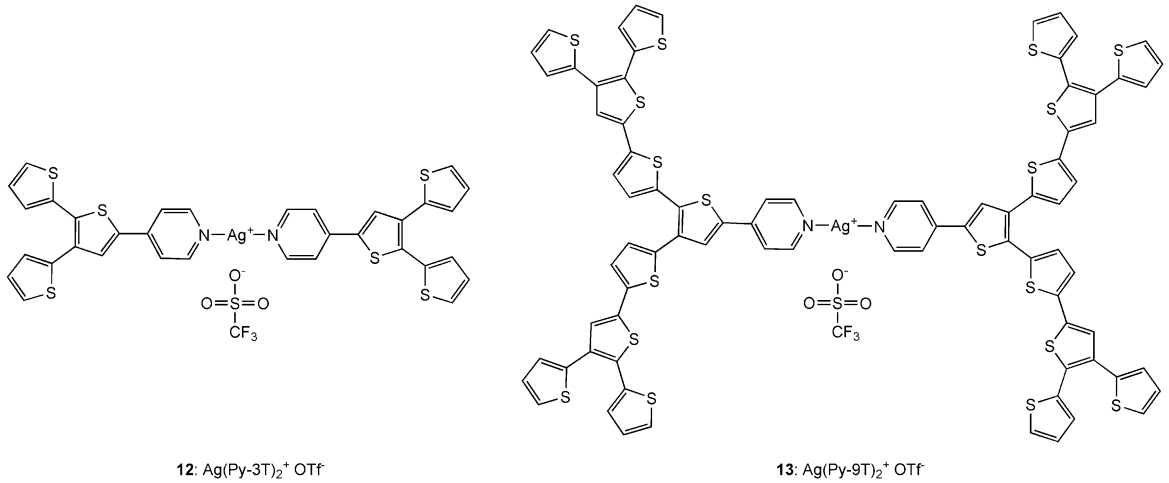

Chart 1 Silver triflate complexes **12** and **13** of the first and second generation pyridine-functionalized DOTs.

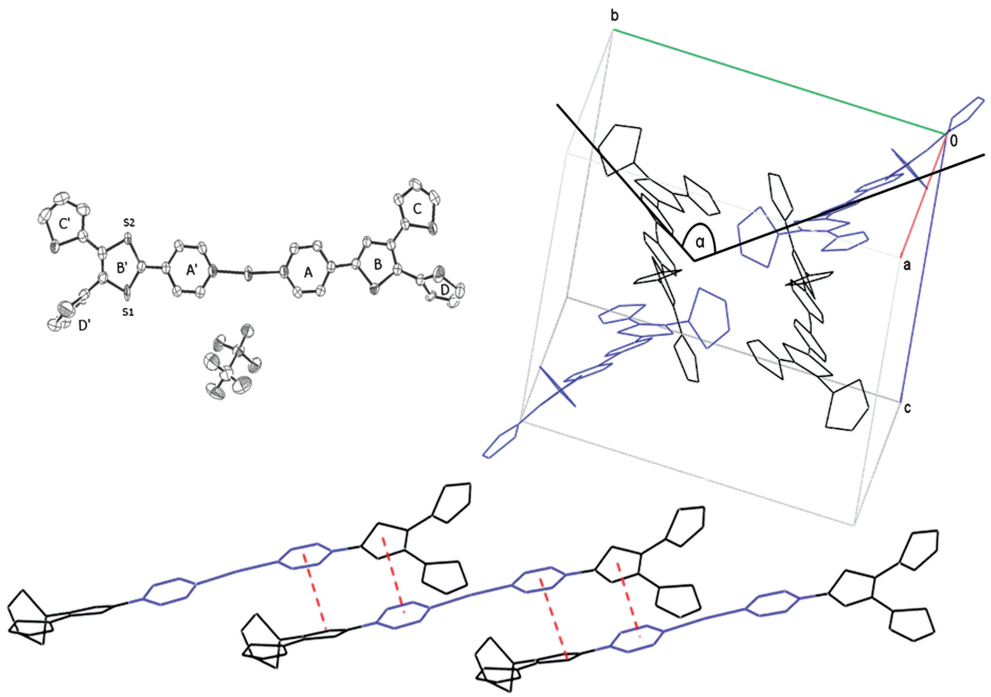

Fig. 2 Top left: ORTEP front view of silver complex **12** in the crystal structure (thermal ellipsoids are drawn at the 50% level of probability). Top right: unit cell of **12** (parallel planes are indicated in blue/black; the angle between the two different planes is designated as α). Bottom: π–π interactions (indicated in red) between pyridine and thiophene rings of different molecules. Counterions and hydrogens are omitted for clarity.

were found in the unit cell, pair-wise arranged parallel to each other. The two pairs were related by a twofold screw axis with an angle of 64° (indicated as α in Fig. 2, top right). The closest distances between parallel arranged molecules were found between electron-rich thiophene and electron-poor pyridine rings. Distance values of 3.32 Å are below the corresponding van der Waals radii which is a clear indication of an effective π–π interaction (Fig. 2, bottom). The pyridine rings draw a torsion angle of approximately 16° to the neighbouring thiophene rings (rings B and B′). The thiophene ring labelled B′ showed a conformational disorder at the sulfur atom, the occupancy being split as 60% for the position S1 and 40% for S2 (Fig. 2, top left). With respect to rings B and B′, the α,β-connected thiophenes are nearly coplanar (10°; rings C and C′), whereas the α,α-connected ones (D and D′) are strongly twisted with dihedral angles of 77.5° and 81.4°, respectively. Each silver ion is coordinated by two pyridine rings and additionally interacts with three sulfur atoms of thiophene rings of two neighbouring complexes. The distance between the silver ion and all three sulfur atoms is approximately 3.36 Å.

Optical properties

In order to evaluate changes in absorption for pyridine and methylpyridinium-functionalized DOTs in comparison to parent DOTs, UV-vis spectra were recorded in dichloromethane solutions. Fluorescence quantum yields, optical band gaps, absorption and emission maxima are given in Table 1. Optical energy gaps correspond to the energy difference of the ground and excited state and therefore correlate to the energy gap between the highest occupied molecular orbital (HOMO) and the lowest unoccupied molecular orbital (LUMO) of the dendrimers. Thus, changes in shape and onset of absorption bands are directly linked to the acceptor strength at the core position of the DOT.

The absorption spectra reveal the following trends: with increasing generation a red-shift and strong increase in intensity of the absorption corresponding to the π–π* transition is observed (Py-*n*T **4**, **7** and **10**). The reason is the elongation of the π-conjugated system. Compared to the parent non-functionalized DOTs pyridine induced a strong red-shift in the absorption of *G1* derivative **4** ($\Delta\lambda^{abs}{}_1 = 47$ nm), whereas for higher generations, Py-*n*T **7** and **10**, the effect was only marginal. Furthermore, broadened absorptions can be observed by introduction of pyridine for all three generations causing a red-shift of the absorption onset and thus a decrease in the optical band gap. The emission band was shifted to lower energies and fluorescence quantum yields were lower for Py-*n*T when compared to parent DOTs. Thus, we can conclude that pyridine exerts a rather weak electron-withdrawing effect on the DOT structure.

In order to show the influence of the different acceptors, namely pyridine and methylpyridinium, on non-functionalized DOTs, absorption spectra of various *G2* derivatives, DOT-9T, Py-9T **7** and MePy$^+$-9T **8** are shown as examples in Fig. 3, left. Whereas the absorption band due to the π–π* transition remains unchanged, for methylpyridinium derivative **8** an additional quite intense band appears at lower energies ($\lambda_{max} = 508$ nm). This new band, whose intensity does not significantly change in the series of methylpyridinium-functionalized DOTs MePy$^+$-*n*T **5**, **8** and **11**, was successively red-shifted with increasing generation ($\Delta\lambda^{abs}{}_2 = 65$ nm (*G1* to *G2*) and 93 nm (*G1* to *G3*); Fig. 3, right).

These results clearly demonstrate that the pyridinium unit represents a much stronger acceptor than pyridine itself. The nature of the new band in the absorption spectra which drastically reduces the band gap in pyridinium-functionalized DOTs correlates with a charge transfer state and additional investigations in this respect are presented in the following.

The observed spectroscopic behaviour that is caused by the strong methylpyridinium acceptor is corroborated by semi-empirical calculations. The quantum-chemical Austin Model 1 (AM1) method under unrestricted Hartree–Fock conditions was used to analyse the electron distribution in the frontier orbitals of

Table 1 UV-vis absorption data of pyridine-functionalized DOTs **4**, **7**, **10** (Py-*n*T) and methylpyridinium-functionalized DOTs **5**, **8**, **11** (MePy$^+$-*n*T) in comparison to parent non-functionalized DOTs (DOT-*n*T) in dichloromethane ($c \approx 1.0 \times 10^{-5}$ mol L^{-1})

Compound	$\lambda^{abs}{}_1$ [nm] (ε [L mol^{-1} cm^{-1}])	$\lambda^{abs}{}_2$ [nm] (ε [L mol^{-1} cm^{-1}])	$\lambda^{em}{}_{max}$ [nm]	Φ_f [%]	$E^{opt}{}_g$ [eV]
MePy$^+$-3T **5**	297 (11500)	442 (21000)	560	1.1 ± 0.7[c]	2.45
Py-3T **4**	284 (18500)	349 (12700)	452	2.1 ± 0.6[c]	3.07
DOT-3T[e]	302 (9200)		440	10	3.47
MePy$^+$-9T **8**	374 (37100)	507 (22100)	[b]	<1[d]	2.03
Py-9T **7**	375 (48300)		545	5.8 ± 0.1[d]	2.54
DOT-9T[e]	373 (37500)		522	12	2.67
MePy$^+$-21T **11**	390 (87900)	535 (25600)[a]	[b]	<1[d]	1.96
Py-21T **10**	385 (101600)		563	11.2 ± 0.2[d]	2.34
DOT-21T[f]	383 (90600)		547	[g]	2.45

[a] Shoulder. [b] Only weak emission from the π–π* transition. [c] Determined against 9,10-diphenylanthracene ($\Phi_f = 88\%$ in ethanol).[40] [d] Determined against fluorescein ($\Phi_f = 92\%$ in 0.1 M NaOH).[41] [e] Values taken from ref. 24. [f] Not published results. [g] Not determined.

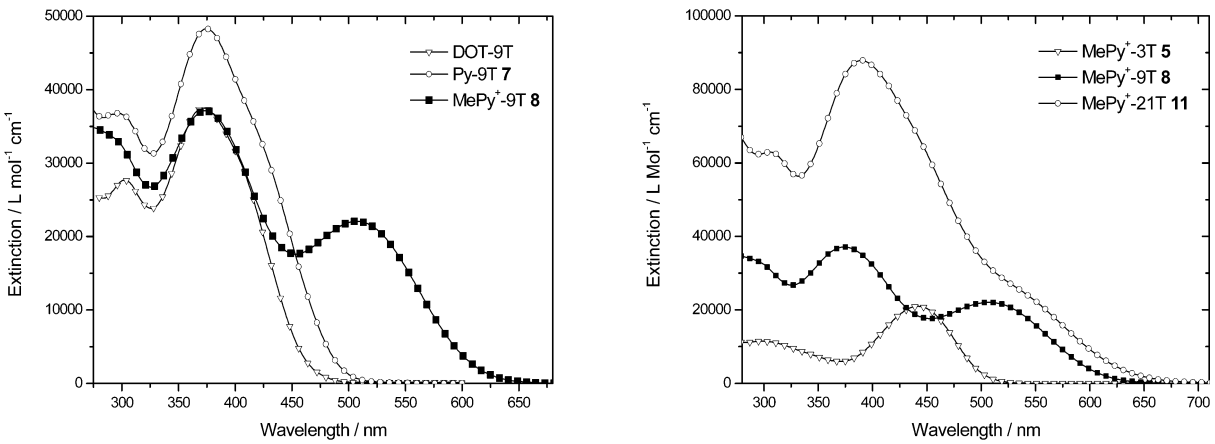

Fig. 3 UV-vis spectra of *G2*-derivatives DOT-9T, Py-9T **7** and MePy$^+$-9T **8** in dichloromethane (left). UV-vis spectra of methylpyridinium-functionalized DOTs MePy$^+$-*n*T **5**, **8** and **11** (*G1* to *G3*; right); $c \approx 1.0 \times 10^{-5}$ mol L^{-1}.

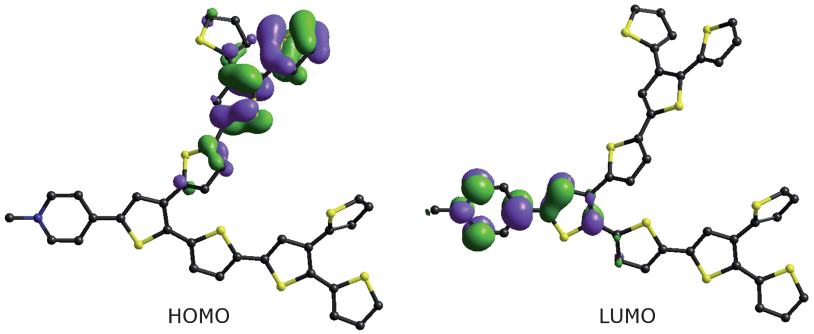

Fig. 4 Semiempirically calculated HOMO (left) and LUMO (right) of methylpyridinium derivative MePy$^+$-9T **8** (carbons in black, nitrogens in blue and sulfurs in yellow, hydrogens omitted for clarity).

MePy$^+$-9T **8** (Fig. 4). Electron density of HOMO and HOMO − 1 is located at the branched quaterthiophene arms, whereas density of LUMO and LUMO + 1 is located at the methylpyridinium acceptor unit including a part of the adjacent thiophene ring. Consequently, electronic transitions between those levels in **8** imply a charge transfer character. In contrast, in the case of the pyridine derivative Py-9T **7** HOMO and LUMO are spread over the whole molecule (not shown), which is in good agreement with the absence of any additional red-shifted band in their absorption spectra.

The charge transfer (CT) character of the low energy absorption band in MePy$^+$-9T **8** has been further investigated in solvents of different polarity. Fig. S1 (ESI†) shows absorption spectra of **8** in four different solvents (cyclohexane, benzene, tetrahydrofuran, dimethyl sulfoxide) of polarities between $\varepsilon = 0.2$ and $\varepsilon = 7.2$. Chlorinated solvents were excluded in order to avoid extra modifications due to distinct polarizability.[42,43] As expected for charged species, a hypsochromic response can be observed due to better stabilization of the charged ground state of MePy$^+$-9T against the excited state for increased solvent polarity. Moreover, the fluorescence of the pyridinium derivatives is nearly fully quenched, which supports the CT character of the low energy absorption band.

Band gaps of the various series were determined at the absorption edge of the low energy side of the π–π^* transitions. In each series, it is evident that the band gaps decrease with increasing size of the dendrons. The same trend is noted for increasing acceptor strength and pyridinium salt **11** (MePy$^+$-21T) exhibits the smallest gap of 1.96 eV.

Redox properties

Whereas optical measurements can be correlated to energy differences of the frontier orbitals, oxidation and reduction potentials provide additional information on the absolute positions of HOMO and LUMO levels which are particularly important for fabrication of solar cells. Therefore, cyclic voltammograms (CV) were measured of the three series of DOTs in dichloromethane or dimethylformamide (DMF) with tetrabutylammonium hexafluorophosphate (TBAHFP) as electrolyte. The data were verified by differential pulse voltammetry (DPV). In general, reduction waves were reversible for all compounds indicating stable radical anions or dianions. In contrast, oxidations were typically quasi- or irreversible due to the fact that the DOT units possess reactive α-positions at the peripheral thiophene rings which lead to coupling reactions of the generated radical cations. As representative examples, CVs of the second generation DOTs Py-9T **7** and MePy$^+$-9T **8** are shown in Fig. 5. First reduction and oxidation potentials, corresponding HOMO and LUMO levels as well as electrochemical band gaps are given in Table 2.

As expected, the reduction potentials shifted to more positive values and the compounds became easier to reduce with increasing size of the dendrons. With increasing size of the DOT

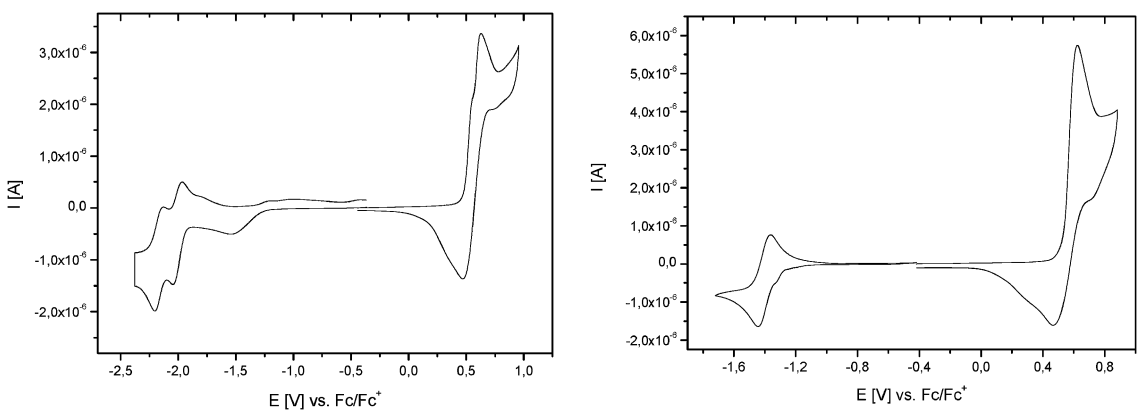

Fig. 5 Cyclic voltammograms of pyridine-DOT Py-9T **7** (left) and pyridinium-DOT MePy$^+$-9T **8** (right) in dichloromethane/TBAHFP (0.1 M) at 100 mV s^{-1} ($c = 1.0 \times 10^{-3}$ mol L^{-1}).

Table 2 Electrochemical properties of Py-*n*T and MePy$^+$-*n*T in comparison to parent DOT-*n*T

Compound	E^0_{red1} [V]	E^0_{ox1} [V]	HOMO [eV][e]	LUMO [eV][e]	E_g^{el} [eV][f]
MePy$^+$-3T **5**	−1.50[a,c]	0.94[a,d]	−5.98	−3.68	2.30
Py-3T **4**	−2.23[b,c]	0.91[a,c]	−5.90	−2.96	2.94
DOT-3T	−2.66[b,d]	0.88[a,d]	−5.84	−2.47	3.37
MePy$^+$-9T **8**	−1.40[a,c]	0.59[a,d]	−5.63	−3.78	1.85
Py-9T **7**	−2.00[b,c]	0.61[a,c]	−5.61	−3.20	2.41
DOT-9T	−2.19[b,d]	0.57[a,d]	−5.62	−3.02	2.53
MePy$^+$-21T **11**	−1.39[a,c]	0.41[a,d]	−5.45	−3.80	1.65
Py-21T **10**	−1.95[b,c]	0.41[a,d]	−5.47	−3.34	2.13
DOT-21T[g]	−2.06[a,c]	0.42[a,d]	−5.52	−3.05	2.34

[a] Measured in dichloromethane/TBAHPF (0.1 M), c = 1.0 × 10^{-3} mol L^{-1}, 295 K, v = 100 mV s^{-1}, potentials *vs.* Fc/Fc$^+$. [b] Measured in DMF/TBAHFP (0.1 M), c = 1.0 × 10^{-3} mol L^{-1}, 295 K, v = 100 mV s^{-1}, *vs.* Fc/Fc$^+$. [c] Values verified by DPV measurement. [d] Determined at $I^0 = 0.855 I_p$.[44] [e] Calculated from E^{onset}_{red1} and E^{onset}_{ox1} set E_{HOMO}(Fc/Fc$^+$) = −5.1 eV.[45] [f] Determined as the difference of the onset of the oxidation and reduction waves. [g] Values from ref. 25.

units in each series, oxidation is facilitated and potentials fall due to increased π-conjugation as well. However, differences and trends are not obvious when compounds of the same generation with different acceptor character are regarded. This definitely results from the localization of the HOMO on the DOT unit (*vide infra*). Band gaps of the various series were determined from the differences of the onset potentials of reduction and oxidation and were somewhat smaller than the optically determined band gaps. With respect to structural changes the trends, however, are identical. Thus, pyridinium salt **11** (MePy$^+$-21T) exhibited the smallest gap of 1.65 eV.

Bulk heterojunction solar cells

HOMO/LUMO levels of pyridinium salts **8** and **11** were promising for application in solution-processed bulk heterojunction solar cells (BHJSCs). HOMO/LUMO energy levels of **8** and **11** are close to the proposed ideal donor material values mentioned in the recent review by Fréchet about BHJSCs.[46] Non-functionalized parent DOTs showed good performance in this type of organic solar cell and efficiencies up to 1.72% were obtained.[25] Compared to the parent compounds, our novel materials showed a red-shift of the absorption and a smaller band gap due to an additional CT band. It was already demonstrated for other donor materials that CT bands can contribute to the photoresponse and incident photon to current efficiency (IPCE) in BHJSCs. In some cases, an increase of the open-circuit voltage was noticed.[47–50]

Therefore, we prepared BHJSCs comprising active films made from chlorobenzene solutions of *G2*- and *G3*-pyridinium salts MePy$^+$-9T **8** and MePy$^+$-21T **11** as donor and soluble fullerene derivative [6,6]-phenyl-C_{61}-butyric acid methyl ester ($PC_{61}BM$) as acceptor. While MePy$^+$-9T **8** was mixed with $PC_{61}BM$ in the ratio 1:2, the best results for MePy$^+$-21T **11** were obtained for a ratio of 1:4. A transparent indium tin oxide (ITO) electrode was covered with poly(3,4-ethylenedioxythiophene):polystyrene sulfonic acid (PEDOT:PSS). For all cells investigated, thicknesses of the active layer were between 60 nm and 70 nm. Devices comprised the overall layer sequence: glass/ITO/PEDOT:PSS/MePy-*n*T$^+$ + $PC_{61}BM$/LiF/Al. *J–V* characteristics were measured under 100 mW cm^{-2} simulated solar light under standard AM1.5G conditions. Data are summarized in Table 3 and compared to the parent DOTs of the same size and generation.[25] Comparison of important parameters of solar cells showed for both series the trend that with higher generation and increasing size of the donor molecules the open circuit voltage V_{OC}, short-circuit current J_{SC}, IPCE and power conversion efficiency increase. Comparison of pyridinium- to non-functionalized derivatives revealed that V_{OC} quite drastically drops and as a consequence efficiencies drop as well to 0.27% for *G2*-**8** and to 0.45% for *G3*-derivative **11** which are about half of the values for the parent DOTs. For J_{SC} and fill factor FF no clear trend was seen. Typically, V_{OC} becomes smaller when the HOMO level of the donor is raised and the energy difference to the LUMO of the acceptor becomes smaller. However, in our case the HOMO levels of acceptor-substituted compounds **8** and **11** were only marginally different from those of the parent DOTs (Table 2). Possible reasons for this unexpected result could come from problems in charge transport for the charged compounds and/or an unfavourable morphology of the active layer resulting in enhanced charge recombination. Corresponding *J–V* curves for pyridinium-functionalized DOTs **8** and **11** are presented in Fig. 6, left, and incident photon to current efficiency (IPCE) curves of *G2*-pyridinium salt **8** and parent DOT-9T in Fig. 6, right. An increase in photocurrent in the region of 470 nm to 600 nm was detected for **8** indicating a contribution of the ICT-band to the photocurrent. For this pair of compounds J_{SC} raises from 1.42 mA cm^{-2} for DOT-9T to 1.98 mA cm^{-2} for MePy$^+$-9T **8**.

Table 3 Characterization of bulk heterojunction solar cells containing MePy$^+$-*n*T:$PC_{61}BM$ as active layer in comparison to parent DOT-*n*T

Compound	Ratio	V_{OC} [V]	J_{SC} [mA cm^{-2}]	FF	EQE_{max} @ wavelength [nm]	$\eta_{AM1.5}$
8 (MePy$^+$-9T)	1:2	0.42	1.98	0.32	19% @ 440	0.27
DOT-9T	1:4	1.06	1.42	0.31	20% @ 450	0.46
11 (MePy$^+$-21T)	1:4	0.60	2.35	0.32	24% @ 460	0.45
DOT-21T	1:4	0.99	2.64	0.37	30% @ 450	0.96

Although the efficiencies of these BHJSCs were rather moderate and not among the best values that can be achieved with highly optimized donor materials, these compounds demonstrate that charged organic molecules can successfully be implemented in BHJSCs and that CT absorptions due to a donor–acceptor character of the active component contribute to the performance of this type of solar cell. Charged cyanine dyes have already been tested as donor and acceptor materials in BHJSCs, however, no power conversion efficiencies were given.[51,52] Also Jørgensen *et al.* have prepared a cyanine oligo *p*-phenylenevinylene derivative that was used in organic solar cells.[53] No efficiency was stated but both the short circuit current density of 1.7 × 10^{-3} mA cm^{-2} and the open circuit voltage of 0.022 V were very low.

3 Conclusion

Novel core-functionalized dendritic oligothiophenes (DOTs) bearing pyridine (Py-*n*T) or methylpyridinium acceptors

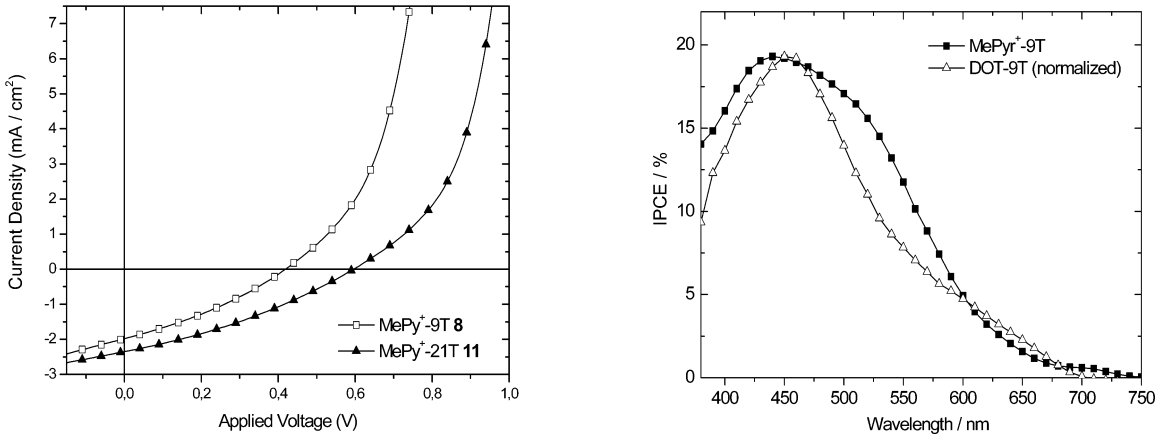

Fig. 6 *J–V* curves of BHJSCs illuminated under standard conditions (AM1.5G; 100 mW cm^{-2}) comprising MePy⁺-9T:$PC_{61}BM$ (1:2) and MePy⁺-21T:$PC_{61}BM$ (1:4) as active layer (left). IPCE curves of pyridinium salt MePy⁺-9T **8** compared to parent DOT-9T (normalized, right).

(MePy⁺-*n*T) have been synthesized up to the third generation. The complexing ability of the pyridine unit in the Py-*n*T series was used to prepare corresponding divalent silver complexes as interesting novel materials. Characterization of the optical properties of the acceptor-functionalized DOTs revealed bathochromic shifts in the absorption spectra. In the case of MePy⁺-*n*T the appearance of a new band at low energies, which can be attributed to an intramolecular charge transfer transition, was found. Quantum chemical calculations corroborate CT states showing the distinct localization of the electron density for the frontier orbitals (HOMO on the thiophene branches and LUMO on the acceptor pyridinium unit). The optical properties strongly change in the series on going from parent DOT-*n*T to Py-*n*T and to MePy⁺-*n*T due to the gradual increase in acceptor strength. The same trends and structure–property relationships were found in electrochemical measurement. Thus, reduction of the dendrons was facilitated with increasing acceptor strength, size and conjugation within the molecule. Band gaps also follow the same trends. The novel donor–acceptor systems pyridinium salts MePy⁺-*n*T **8** and **11** were implemented with fullerene derivative $PC_{61}BM$ as the acceptor in bulk heterojunction solar cells (BHJSC). Although a contribution of the CT band to the photoresponse was proven, lower efficiencies (up to 0.45%) compared to the corresponding parent non-functionalized DOTs were obtained.

4 Experimental section

Details of the solar cell device fabrication, the analytics and used chemicals can be found in the ESI.†

Syntheses

4-[5,5″-Bis(trimethylsilyl)-[2,2′;3′,2″]terthien-5′-yl]-pyridine (2, Py-3T-Si). 4-Iodopyridine (641 mg, 3.0 mmol, 1.0 eq.), boronic acid ester B-3T-Si **1** (1.56 g, 3.0 mmol, 1.0 eq.), $Pd_2(dba)_3 \cdot CHCl_3$ (31.1 mg, 0.03 mmol, 0.01 eq.) and $HP(tBu)_3BF_4$ (17.4 mg, 0.06 mmol, 0.02 eq.) were dissolved in well degassed tetrahydrofuran (20 mL). A well degassed K_3PO_4 solution (6.0 mL, 12.0 mmol, 2 M) was added dropwise. The reaction mixture was stirred for 5 h at room temperature. Then water (10 mL) was added and the mixture extracted three times with diethyl ether. The combined organic extracts were washed with brine and then dried over sodium sulfate. The solvent was removed by rotary evaporation and the residue purified by column chromatography (silica, dichloromethane : ethyl acetate = 5 : 1) to provide 1.36 g Py-3T-Si **2** (2.90 mmol, 97%) as a yellow oil. ^{1}H NMR ([D_8]THF, 400 MHz): δ = 8.55 (dd, ^3J = 4.51 Hz, ^4J = 1.65 Hz, 2H, PyH), 7.54 (dd, ^3J = 4.51 Hz, ^4J = 1.65 Hz, 2H, PyH), 7.73 (s, 1H, ThH), 7.21 (d, ^3J = 3.47 Hz, 1H, ThH), 7.18 (m, 3H, ThH), 0.30 (s, 9H, $SiMe_3$), 0.30 (s, 9H, $SiMe_3$); ^{13}C NMR ($CDCl_3$, 100 MHz): δ = 150.3, 142.6, 141.8, 141.0, 140.5, 139.4, 138.6, 134.2, 133.4, 132.6, 128.8, 128.2, 127.9, 119.4, −0.1, −0.1; MS (EI): *m*/*z* 471 ([M + H]⁺, 35), 470([M]⁺, 100), 457 (15), 456 (29), 455 (22), 73 (29); elemental analysis: calc. (%) for $C_{23}H_{27}NS_3Si_2$: C 58.80; H 5.79; N 2.98; found: C 58.58, H 5.88; N 2.91.

4-[5,5″-Diiodo-[2,2′;3′,2″]terthien-5′-yl]-pyridine (3, Py-3T-I). To a solution of Py-3T-Si **2** (0.47 g, 1.0 mmol, 1.0 eq.) in dry tetrahydrofuran (10 mL) a solution of iodine chloride (0.97 g, 6.0 mmol, 6.0 eq.) in dry tetrahydrofuran (5 mL) was added slowly *via* a syringe at room temperature. After two hours a $NaHCO_3$ solution (10 mL) was added. To remove the excess of iodine chloride a saturated Na_2SO_3 solution was slowly added to this mixture till the dark colour disappeared. Some brine was added and the mixture was extracted three times with dichloromethane. The organic extracts were washed with brine and dried over sodium sulfate. The solvent was removed by rotary evaporation, and the residue was purified by column chromatography (silica, dichloromethane : ethyl acetate = 7 : 1) to provide Py-3T-I **3** (0.55 g, 0.95 mmol, 95%) as a yellow oil. In order to obtain a solid, the product can be dissolved in as little tetrahydrofuran as possible and precipitated into methanol. After filtration, the product is recovered as a yellow powder. Mp 154°C; ^{1}H NMR ([D_8]THF, 400 MHz): δ = 8.56 (dd, ^3J = 4.51 Hz, ^4J = 1.62 Hz, 2H, PyH), 7.72 (s, 1H, ThH), 7.54 (dd, ^3J = 4.51 Hz, ^4J = 1.62 Hz, 2H, PyH), 7.24 (d, ^3J = 3.77 Hz, 1H, ThH), 7.23 (d, ^3J = 3.76 Hz, 1H, ThH), 6.93 (d, ^3J = 3.76 Hz, 1H, ThH), 6.89 (d, ^3J = 3.72 Hz, 1H, ThH); ^{13}C NMR ([D_8]THF, 100 MHz): δ = 151.3, 143.0, 140.8, 140.4, 140.4, 138.2, 137.9, 133.4, 132.7, 130.7, 129.7, 128.5, 119.8, 77.5, 75.8; MS (CI): *m*/*z* (%): 578 ([M + H]⁺, 100), 606 ([M + C_2H_5]⁺, 19), 579 ([M + 2H]⁺, 29), 577 ([M]⁺, 59), 452 (34), 451

(70); elemental analysis: calc. (%) for $C_{14}H_8I_2O_2S_3$: C 35.37; H 1.57; N 2.43; found: C 35.47; H 1.62; N 2.37.

4-[2,2′;3′,2″-Terthien-5′-yl]-pyridine (4, Py-3T). Py-3T-Si **2** (95 mg, 0.20 mmol) was dissolved in dichloromethane (3 mL) and trifluoroacetic acid (1 mL) was added dropwise. The solution was stirred for 10 min at room temperature. Then water (10 mL) was added and the product was extracted three times with dichloromethane (10 mL). The organic phase was washed with 1 M NaOH solution (10 mL). The organic phase was dried over sodium sulfate and after purification by column chromatography (silica; DCM : EtOAc = 5 : 1) the product was obtained as a slightly yellow oil. After redissolving the product in tetrahydrofuran and precipitating into a mixture of methanol–water (1 : 1) and subsequent filtration, **4** was obtained as a slightly yellow solid (65 mg, 0.20 mmol, 99%). Mp 103°C; ^{1}H NMR ([D$_6$]DMSO, 400 MHz): δ = 8.61 (m, 2H, PyH), 8.04 (s, 1H, ThH), 7.71–7.73 (m, 2H, PyH), 7.69 (dd, ^3J = 5.11 Hz, ^4J = 1.15 Hz, 1H, ThH), 7.59 (dd, ^3J = 5.10 Hz, ^4J = 1.15 Hz, 1H, ThH), 7.31 (dd, ^3J = 3.56 Hz, ^4J = 1.17 Hz, 1H, ThH), 7.28 (dd, ^3J = 3.58 Hz, ^4J = 1.17 Hz, 1H, ThH), 7.14 (dd, ^3J = 5.11 Hz, ^3J = 3.58 Hz, 1H, ThH), 7.12 (dd, ^3J = 5.10 Hz, ^3J = 3.56 Hz, 1H, ThH); ^{1}H NMR ([D$_8$]THF, 400 MHz): δ = 8.55 (dd, ^3J = 4.47 Hz, ^4J = 1.67 Hz, 2H, PyH), 7.73 (s, 1H, ThH), 7.55 (dd, ^3J = 4.47 Hz, ^4J = 1.67 Hz, 2H, PyH), 7.44 (dd, ^3J = 5.13 Hz, ^4J = 1.19 Hz, 1H, ThH), 7.39 (dd, ^3J = 5.12 Hz, ^4J = 1.19 Hz, 1H, ThH), 7.18 (dd, ^3J = 3.62 Hz, ^4J = 1.17 Hz, 1H, ThH), 7.14 (dd, ^3J = 3.57 Hz, ^4J = 1.19 Hz, 1H, ThH), 7.01 (m, 2H, ThH); ^{13}C NMR ($CDCl_3$, 100 MHz): δ = 150.4, 140.6, 139.0, 136.6, 134.3, 133.6, 132.9, 128.1, 128.0, 127.3, 127.2, 127.2, 127.0, 125.9, 119.5; MS (EI): *m*/*z* 326 ([M + H]$^+$, 26), 325 ([M]$^+$, 100), 280 (16), 69 (8); elemental analysis: calc. (%) for $C_{17}H_{11}NS_3$: C 62.73; H 3.41; N 4.30; found: C 62.77, H 3.69; N 4.14.

***N*-Methyl-4-[2,2′;3′,2″-terthien-5′-yl]-pyridinium trifluoromethane sulfonate (5, MePy$^+$-3T).** In a 10 mL Schlenk tube Py-3T **4** (75 mg, 0.23 mmol, 1.0 eq.) was dissolved in a mixture of dry dichloromethane (1 mL) and dry diethyl ether (2 mL). The solution was cooled with ice and freshly distilled methyl trifluoromethanesulfonate (28.7 μL, 0.25 mmol, 1.1 eq.) was added *via* an Eppendorf pipette. A yellow precipitate formed immediately. The suspension was warmed to room temperature and stirred for 0.5 h. The suspension was precipitated into diethyl ether (10 mL). Under reduced pressure the mixture was concentrated, then filtered and subsequently washed with water and diethyl ether to provide MePy$^+$-3T **5** (105 mg, 0.21 mmol, 93%) as a yellow solid. Mp 161°C; ^{1}H NMR ([D$_6$]DMSO, 400 MHz): δ = 8.90 (d, ^3J = 6.66 Hz, 2H, PyH), 8.43 (s, 1H, ThH), 8.38 (d, ^3J = 6.66 Hz, 2H, PyH), 7.75 (d, ^3J = 4.92 Hz, 1H, ThH), 7.65 (d, ^3J = 4.92 Hz, 1H, ThH), 7.36 (d, ^3J = 3.19 Hz, 1H, ThH), 7.33 (d, ^3J = 3.09 Hz, 1H, ThH), 7.16 (m, 2H, ThH), 4.27 (s, 3H, NCH_3); ^{13}C NMR ([D$_6$]DMSO, 100 MHz): δ = 174.3, 173.2, 165.4, 162.4, 162.4, 161.9, 161.4, 160.1, 157.3, 157.0, 155.8, 155.7, 155.3, 155.2, 149.5, 148.4 (q, $^2J_{C,F}$ = 322.51 Hz, 1C), 74.6; ^{19}F NMR ([D$_6$]DMSO, 376 MHz): δ =77.94 (hexafluorobenzene 0.1 M in $CDCl_3$ set to 162.6); MS (CI): *m*/*z* (%):340 ([M$^+$], 35), 165 (27), 326 ([M − CH_2]$^+$, 100), 354 ([M − CH_2 + C_2H_5]$^+$, 20), 368 ([M + C_2H_5]$^+$, 1); elemental analysis: calc. (%) for $C_{19}H_{14}F_3NO_3S_4$: C 46.61; H 2.88; N 2.86; S 26.20; found: C 46.52, H 2.98; N 2.78; S 25.96.

4-[5,5‴′′′-Bis(trimethylsilyl)-3′,5‴′′′-bis[5-(trimethylsilyl)-2-thienyl][2,2′:5′,2″:5″,2‴:3‴,2⁗:5⁗,2⁗′:4⁗′,2⁗′′-septithien]-5‴-yl]-pyridine (6, Py-9T-Si). To a solution of Py-3T-I **3** (115 mg, 0.20 mmol, 1.0 eq.), boronic acid ester B-3T-Si **1** (228 mg, 0.44 mmol, 2.2 eq.), $Pd_2(dba)_3 \cdot CHCl_3$ (4.14 mg, 4.00 μmol, 0.02 eq.) and $HP(tBu)_3BF_4$ (2.23 mg, 8.00 μmol, 0.04 eq.) were dissolved in well degassed tetrahydrofuran (4 mL). A well degassed K_3PO_4 solution (0.80 mL, 1.60 mmol, 8.0 eq., 2 M) was added dropwise *via* a syringe. The reaction mixture was stirred for 5 h at room temperature. After addition of water (15 mL) the mixture was extracted three times with diethyl ether. The combined organic extracts were washed with brine and then dried over sodium sulfate. The solvent was removed by rotary evaporation and the residue was purified by column chromatography (compound packed on silica, dichloromethane : ethyl acetate = 4 : 1) to provide Py-9T-Si **6** (199 mg, 0.18 mmol, 90%) as an orange-red solid. A powder was formed by precipitating the product from a tetrahydrofuran solution into a methanol–water mixture. After filtration and drying Py-9T-Si **6** is produced as red-orange powder. Mp 181°C; ^{1}H NMR ([D$_8$]THF, 400 MHz): δ = 8.58 (dd, ^3J = 4.58 Hz, ^4J = 1.54 Hz, 2H, PyH), 7.82 (s, 1H, ThH), 7.59 (dd, ^3J = 4.58 Hz, ^4J = 1.54 Hz, 2H, PyH), 7.33 (s, 1H, ThH), 7.31 (s, 1H, ThH), 7.26 (m, 2H, ThH), 7.23 (d, ^3J = 3.83 Hz, 1H, ThH), 7.20 (d, ^3J = 3.78 Hz, 1H, ThH), 7.16 (m, 8H, ThH), 0.29 (s, 36H, $SiMe_3$); ^{13}C NMR ([D$_8$]THF, 100 MHz): δ = 151.2, 142.8, 142.7, 142.6, 142.5, 141.2, 141.1, 140.7, 140.6, 140.4, 140.4, 138.9, 137.7, 136.6, 136.1, 135.6, 135.1, 134.9, 134.1, 133.5, 133.3, 133.3, 133.2, 131.5, 131.1, 130.1, 129.5, 129.4, 129.1, 129.1, 128.8, 128.7, 127.5, 127.1, 125.2, 125.0, 119.8, −0.2, −0.2; MS (MALDI): *m*/*z* 1104.9 [M]$^+$ (calc. for $C_{53}H_{55}NS_9Si_4$: 1105.1); elemental analysis: calc. (%) for $C_{53}H_{55}NS_9Si_4$: C 57.51; H 5.01; N 1.27; found: C 57.63; H 5.10; N 1.19.

4-[3′,5⁗′′-Di-2-thienyl-[2,2′:5′,2″:5″,2‴:3‴,2⁗:5⁗,2⁗′:4⁗′,2‴:-3‴-septithien]-5‴-yl]-pyridine (7, Py-9T). Py-9T-Si **6** (111 mg, 0.10 mmol, 1.0 eq.) was dissolved in THF (5 mL) and tetra-*n*-butylammonium fluoride solution (TBAF) (0.8 mL, 0.8 mmol, 1M) was added dropwise. The solution was stirred for 0.5 h at room temperature. After addition of water (10 mL) the product was extracted three times with dichloromethane (10 mL). The organic phase was washed with 1 M NaOH solution (10 mL) and dried over sodium sulfate. The product was dissolved in as little dichloromethane as possible and was precipitated into methanol. After filtration and drying **7** (81.8 mg, 0.10 mmol, 99%) was produced as an orange powder. Mp 105 °C; ^{1}H NMR ([D$_8$]THF, 400 MHz): δ = 8.57 (dd, ^3J = 4.56 Hz, ^4J = 1.54 Hz, 2H, PyH) 7.80 (s, 1H, ThH), 7.57 (dd, ^3J = 4.56 Hz, ^4J = 1.54 Hz, 2H, PyH), 7.41 (dt, ^3J = 5.14 Hz, ^4J = 1.05 Hz, 2H, ThH), 7.36 (dt, ^3J = 5.12 Hz, ^4J = 1.05 Hz, 2H, ThH), 7.31 (s, 1H, ThH), 7.33 (s, 1H, ThH), 7.25 (d, ^3J = 3.77 Hz, 2H, ThH), 7.22 (d, ^3J = 3.82 Hz, 1H, ThH), 7.19 (d, ^3J = 3.75 Hz, 1H, ThH), 7.13 (m, 2H, ThH), 7.10 (m, 2H, ThH), 6.98 (m, 4H, ThH); ^{13}C NMR ([D$_8$]THF, 100 MHz): δ = 151.3, 140.7, 140.5, 138.8, 137.7, 137.3, 137.2, 136.7, 136.0, 135.6, 135.0, 134.9, 134.1, 133.5, 133.5, 133.2, 131.6, 131.2, 130.0, 129.1, 129.0, 128.6, 128.5, 127.8, 127.8, 127.7, 127.6, 127.6, 127.4, 127.0, 126.6, 126.6, 125.3, 125.1, 119.8; MS (MALDI): *m*/*z* 818.1 [M + H]$^+$ (calc. for $C_{41}H_{24}NS_9$: 817.9); elemental analysis: calc. (%) for $C_{41}H_{23}NS_9$: C 60.18; H 2.83; N 1.71; found: C 59.98; H 2.98; N 1.53.

***N*-Methyl-4-[3′,5‴″-di-2-thienyl-[2,2′:5′,2″:5″,2‴:3‴,2⁗:5⁗,-2‴″:4‴″,2⁗:3⁗-septithien]-5‴-yl]-pyridinium trifluoromethane sulfonate (8, MePy$^+$-9T).** In a 10 mL round bottom flask Py-9T **7** (81.8 mg, 0.10 mmol, 1.0 eq.) was dissolved in dry dichloromethane (3 mL). The solution was cooled with ice and freshly distilled methyl trifluoromethane sulfonate (28.7 μL, 0.13 mmol, 1.3 eq.) was added *via* an Eppendorf pipette. The solution immediately turned red and was stirred for 1 h at room temperature and then precipitated into a mixture of hexane (3 mL) and diethyl ether (3 mL). The solid was filtered off and washed with diethyl ether. After drying under vacuum MePy$^+$-9T **8** (93 mg, 0.09 mmol, 95%) was isolated as a red solid. Mp 153 °C; ^{1}H NMR ([D$_8$]THF, 400 MHz): δ = 8.86 (m, 2H, PyH), 8.24 (m, 2H, PyH), 8.20 (s, 1H, ThH), 7.38 (m, 2H, ThH), 7.32 (m, 2H, ThH), 7.27 (m, 4H, ThH), 7.22 (m, 2H, ThH), 7.07 (m, 4H, ThH), 6.96 (m, 4H, ThH), 4.37 (s, 3H, NCH$_3$); ^{13}C NMR ([D$_8$]THF, 100 MHz): δ = 148.0, 146.6, 139.9, 138.6, 138.2, 137.3, 137.2, 136.1, 135.9, 135.4, 135.3, 135.0, 134.9, 134.8, 134.4, 133.5, 133.5, 133.1, 132.1, 131.4, 131.0, 130.1, 128.6, 128.6, 127.8, 127.8, 127.8, 127.7, 127.7, 127.7, 127.6, 127.1, 126.6, 126.5, 125.5, 125.2, 122.6, 47.6; ^{19}F NMR ([D$_8$]THF, 376 MHz): δ = 79.54 (hexafluorobenzene 0.1M in CDCl$_3$ set to 162.6); MS (MALDI): *m*/*z* 832.1 [M]$^+$ (calc. for $C_{42}H_{26}NS_9$: 832.0); elemental analysis: calc. (%) for $C_{43}H_{26}F_3NO_3S_{10}$: C 52.58; H 2.67; N 1.43; S 32.64; found: C 52.57; H 2.97; N 1.52; S 32.47.

4-[3′,5⁗⁗⁗⁗⁗⁗⁗⁗-Di-2-thienyl-3‴,5⁗⁗⁗⁗⁗⁗-bis[5′-(2-thienyl)[2,2′:4′,2″-terthien]-5-yl][2,2′:5′,2″:5″,2‴:5‴,2⁗:5⁗,2⁗⁗⁗⁗:3⁗⁗⁗⁗,2‴:3‴:5‴:3‴,-2⁗⁗⁗⁗⁗:4⁗⁗⁗⁗⁗,2⁗⁗⁗⁗⁗⁗:5⁗⁗⁗⁗⁗,2⁗⁗⁗⁗⁗⁗⁗⁗:4⁗⁗⁗⁗⁗⁗⁗⁗,2⁗⁗⁗⁗⁗⁗⁗⁗⁗⁗]undecithien-5⁗⁗⁗⁗⁗-yl]-pyridine (10, Py-21T). Py-3T-I **3** (90 mg, 156 μmol, 1.0 eq.), B-9T-Si **9** (396 mg, 343 μmol, 2.2 eq.), Pd$_2$(dba)$_3$·CHCl$_3$ (3.23 mg, 3.12 μmol, 0.02 eq.) and HP(*t*Bu)$_3$BF$_4$ (1.81 mg, 6.24 μmol, 0.04 eq.) were dissolved in well-degassed tetrahydrofuran (10 mL). A well-degassed K_3PO_4 solution (0.83 mL, 1.25 mmol, 8.0 eq., 1.5 M) was added dropwise *via* syringe. The reaction mixture was stirred for 5 h at room temperature. The product was extracted three times with dichloromethane. The organic phase was washed with brine and dried over sodium sulfate. The solvents were removed and the resulting solid redissolved in tetrahydrofuran (2 mL). Size exclusion chromatography (SEC) (Bio-Beads® S-X-1, eluent tetrahydrofuran) was performed. With the collected second band column chromatography (silica; dichloromethane with 1% Et$_3$N) was performed. The solvents were removed and the resulting solid redissolved in tetrahydrofuran (5 mL). A solution of TBAF (2.5 mL, 2.5 mmol, 16 eq., 1 M) was added dropwise and the mixture stirred for another 2 h. After addition of water (10 mL) the product was extracted three times with dichloromethane. The organic phase was washed with brine and dried over sodium sulfate. The solvents were removed and the resulting solid redissolved in tetrahydrofuran (2 mL). Methanol was added till the product precipitated completely. The solid was filtered off and washed with water, methanol and diethyl ether subsequently. Py-21T **10** (197 mg, 0.11 mmol, 70%) was provided as a red solid. Mp 142 °C; ^{1}H NMR ([D$_8$]THF, 400 MHz): δ = 8.58 (dd, ^3J = 4.54 Hz, ^4J = 1.59 Hz, 2H, PyH), 7.87 (s, 1H, ThH), 7.59 (dd, ^3J = 4.54 Hz, ^4J = 1.59 Hz, 2H, PyH), 7.40 (m, 6H, ThH), 7.34 (m, 4H, ThH), 7.32 (s, 1H, ThH), 7.31 (m, 3H, ThH), 7.29 (s, 1H, ThH), 7.29 (s, 1H, ThH), 7.26 (d, ^3J = 3.83 Hz, 1H, ThH), 7.32 (m, 5H, ThH), 7.17 (m, 4H, ThH), 7.12 (m, 4H, ThH), 7.09 (m, 4H, ThH), 6.98 (m, 8H, ThH); ^{13}C NMR ([D$_8$]THF, 100 MHz): δ = 151.3, 140.7, 140.5, 138.6, 138.4, 138.4, 137.5, 137.5, 137.3, 137.3, 136.9, 136.7, 136.6, 136.3, 136.1, 135.7, 135.7, 135.1, 135.0, 134.4, 134.3, 134.2, 133.4, 133.4, 133.4, 133.3, 132.9, 132.9, 131.5, 131.4, 131.2, 131.1, 130.8, 130.1, 129.7, 129.6, 129.2, 129.1, 129.0, 129.0, 128.5, 128.5, 127.8, 127.8, 127.7, 127.7, 127.6, 127.6, 127.3, 127.2, 127.0, 126.9, 126.6, 126.5, 125.5, 125.3, 125.2, 125.0, 119.8; MS (MALDI): *m*/*z* 1800.9 [M]$^+$ (calc. for $C_{89}H_{47}NS_{21}$: 1800.8); elemental analysis: calc. (%) for $C_{89}H_{47}NS_{21}$: C 59.26; H 2.63; N 0.78; found: C 59.16; H 2.78; N 0.77.

***N*-Methyl-4-[3′,5⁗⁗⁗⁗⁗⁗⁗⁗-di-2-thienyl-3‴,5⁗⁗⁗⁗⁗-bis[5′-(2-thienyl)-[2,2′:4′,2″-terthien]-5-yl][2,2′:5′,2″:5″,2‴:5‴,2⁗:5⁗,2⁗⁗⁗⁗:3⁗⁗⁗⁗,-2‴:3‴:5‴:3‴,2⁗⁗⁗⁗⁗:4⁗⁗⁗⁗⁗,2⁗⁗⁗⁗⁗⁗:5⁗⁗⁗⁗⁗,2⁗⁗⁗⁗⁗⁗⁗⁗:4⁗⁗⁗⁗⁗⁗⁗⁗,2⁗⁗⁗⁗⁗⁗⁗⁗⁗⁗]undecithien-5⁗⁗⁗⁗⁗-yl]-pyridinium trifluoromethane sulfonate (11, MePy$^+$-21T).** In a 25 mL round bottom flask Py-21T **10** (80.0 mg, 44.4 μmol, 1.0 eq.) was dissolved in dry 1,4-dioxane (8 mL). The solution was cooled with ice till it was solid and freshly distilled methyl trifluoromethane sulfonate (10.0 μL, 88.7 μmol, 2.0 eq.) was added *via* an Eppendorf pipette. The solution was stirred for 1 h at room temperature. After the solvent has been removed the solid was dissolved in as little dichloromethane as possible and precipitated into methanol. The solid was filtered off and washed with diethyl ether. The solid was dried under vacuum and MePy$^+$-21T **11** (80 mg, 40.7 μmol, 92%) was provided as a black solid. Mp 201 °C; ^{1}H NMR ([D$_8$]THF, 400 MHz): δ = 8.79 (d, ^3J = 5.60 Hz, 2H, PyH), 8.14 (d, ^3J = 5.60 Hz, 2H, PyH), 8.12 (s, 1H, ThH), 7.32 (m, 4H, ThH), 7.24–7.28 (m, 5H, ThH), 7.23 (m, 4H, ThH), 7.14–7.18 (m, 4H, ThH), 7.06 (m, 4H, ThH), 6.97–7.03 (m, 13H, ThH), 6.91 (m, 8H, ThH), 4.32 (s, 3H, NCH$_3$); ^{13}C NMR ([D$_8$]THF, 125 MHz): δ = 147.9, 146.4, 139.8, 138.8, 138.4, 138.3, 138.1, 137.5, 137.4, 137.4, 137.3, 137.3, 136.7, 136.5, 136.2, 136.1, 135.8, 135.8, 135.8, 135.4, 135.1, 135.1, 134.3, 134.2, 134.2, 133.4, 133.3, 133.3, 133.3, 133.1, 132.8, 131.6, 131.5, 131.4, 131.2, 131.1, 131.1, 130.9, 130.3, 130.2, 129.6, 129.1, 129.0, 128.5, 128.5, 127.8, 127.7, 127.6, 127.6, 127.2, 127.1, 127.1, 126.9, 126.8, 126.5, 126.4, 125.5, 125.3, 125.1, 125.0, 122.5, 47.6; MS (MALDI): *m*/*z* 1816.1 [M]$^+$ (calc. for $C_{90}H_{50}NS_{21}$: 1815.8); elemental analysis: calc. (%) for $C_{91}H_{50}F_3NO_3S_{22}$: C 55.54; H 2.56; N 0.71; found: C 55.56; H 2.74; N 0.70.

Bis-[4-[2,2′;3′,2″-terthien-5′-yl]-pyridine]-silver(I) trifluoromethane sulfonate (12, Ag(Py-3T)$_2^+$OTf$^-$). Py-3T **4** (51.0 mg, 0.16 mmol, 2.0 eq.) was dissolved in THF (1 mL). A solution of silver(I) trifluoromethane sulfonate (20.1 mg, 0.08 mmol, 1.0 eq.) in 1 mL acetonitrile was added in the dark and the resulting mixture was stirred overnight. Diethyl ether was added to precipitate the complex. The solid was filtered off and washed with water and diethyl ether subsequently to provide silver complex **12** (69.2 mg, 0.08 mmol, 97%) as a yellow solid. In order to gain single crystals the product was recrystallized from acetonitrile. Mp 210 °C (decomposition); ^{1}H NMR ([D$_6$]DMSO, 400 MHz): δ = 8.62 (m, 4H, PyH), 8.06 (s, 2H, ThH), 7.76 (dd, ^3J = 4.67 Hz, ^4J = 1.52 Hz, 4H, ThH), 7.69 (m, 2H, PyH), 7.59 (m, 2H, PyH), 7.31 (dd, ^3J = 3.54 Hz, ^4J = 1.07 Hz, 2H, ThH), 7.28 (dd, ^3J = 3.54 Hz, ^4J = 1.07 Hz, 2H, ThH), 7.11–7.15 (m, 4H, ThH); ^{13}C NMR

([D_6]DMSO, 100 MHz): δ = 150.69, 139.91, 138.37, 135.64, 133.17, 133.05, 132.29, 129.09, 128.86, 128.73, 127.81, 127.59, 127.36, 127.10, 119.52; ^{19}F NMR ([D_6]DMSO, 376 MHz): δ = 77.09 (hexafluorobenzene 0.1 M in $CDCl_3$ set to 162.6); MS (MALDI): *m/z* 757.1 $[M\text{-}OTf]^+$ (calc. for $C_{34}H_{22}AgN_2S_6$: 756.9; also fragments of the complex can be observed); single crystal X-ray data are given at the end of the experimental section and are deposited at the Cambridge Structural Database (CSD) with the deposition number CCDC 711680.

Bis-[4-[3′,5′′′′-di-2-thienyl-[2,2′:5′,2′′:5′′,2′′′:3′′′,2′′′′:5′′′′,2′′′′′:4′′′′′,2′′′′′′:3′′′′′′-septithien]-5′′′′′′-yl]-pyridine]-silver(I) trifluoromethane sulfonate (13, $Ag(Py\text{-}9T)_2^+OTf^-$). Py-9T **7** (75.0 mg, 91.7 μmol, 2 eq.) was dissolved in THF (1 mL). A solution of silver(I) trifluoromethane sulfonate (11.8 mg, 45.8 μmol, 1.0 eq.) in 1 mL acetonitrile was added in the dark and the resulting mixture was stirred overnight. All solvents were removed under reduced pressure and the resulting solid was redissolved in THF (2 mL). The solution was precipitated into diethyl ether (8 mL) and subsequently methanol (5 mL) was added. The mixture was concentrated under reduced pressure to complete the precipitation. The solid was filtered off and washed with methanol and diethyl ether to provide silver complex **13** (80.0 mg, 42.2 μmol, 92%) as an orange solid. Mp 149 °C (decomposition); ^{1}H NMR ([D_8]THF, 400 MHz): δ = 8.70 (m, 4H, PyH), 7.73 (s, 2H, ThH), 7.51–7.53 (m, 4H, PyH), 7.33–7.36 (m, 4H, ThH), 7.29–7.32 (m, 4H, ThH), 7.17–7.21 (m, 4H, ThH), 7.13–7.14 (m, 2H, ThH), 7.08–7.11 (m, 6H, ThH), 7.00–7.04 (m, 8H, ThH), 6.89–6.95 (m, 8H, ThH); ^{13}C NMR ([D_8]THF, 100 MHz): δ = 152.13, 143.01, 139.09, 138.71, 137.81, 137.39, 137.27, 136.22, 136.06, 135.56, 135.09, 135.00, 133.80, 133.44, 133.41, 131.78, 131.26, 130.85, 130.83, 130.27, 129.35, 128.59, 128.55, 127.82, 127.76, 127.74, 127.70, 127.65, 127.62, 127.42, 126.97, 126.60, 126.54, 125.28, 125.06, 120.54; ^{19}F NMR ([D_6]DMSO, 376 MHz): δ = 77.19 (hexafluorobenzene 0.1 M in $CDCl_3$ set to 162.6); elemental analysis: calc. (%) for $C_{83}H_{46}AgF_3N_2O_3S_{19}$: C 52.65; H 2.45; N 1.48; found: C 52.52; H 2.68; N 1.46.

Acknowledgements

This work was supported by the German Science Foundation (DFG) in the framework of the Collaborative Research Center (SFB) 569. We would like to thank the Fonds der Chemischen Industrie for financial support and Dr E. Mena-Osteritz (University of Ulm) and Dr M. Wienk (TU Eindhoven) for help concerning calculations and solar cells, respectively.

References

1 S. K. Deb, T. M. Maddux and L. Yu, *J. Am. Chem. Soc.*, 1997, **119**, 9079–9080.
2 J. S. Moore, *Acc. Chem. Res.*, 1997, **30**, 402–413.
3 L. Gong, Q. Hu and L. Pu, *J. Org. Chem.*, 2001, **66**, 2358–2367.
4 A. J. Berresheim, M. Müller and K. Müllen, *Chem. Rev.*, 1999, **99**, 1747–1785.
5 P. R. L. Malenfant, L. Groenendaal and J. M. J. Fréchet, *J. Am. Chem. Soc.*, 1998, **120**, 10990–10991.
6 J. J. Apperloo, R. A. J. Janssen, P. R. L. Malenfant, L. Groenendaal and J. M. J. Fréchet, *J. Am. Chem. Soc.*, 2000, **122**, 7042–7051.
7 A. Adronov, P. R. L. Malenfant and J. M. J. Fréchet, *Chem. Mater.*, 2000, **12**, 1463–1472.
8 A. Cravino, S. Roquet, O. Aleveque, P. Leriche, P. Frere and J. Roncali, *Chem. Mater.*, 2006, **18**, 2584–2590.
9 L. L. Miller, Y. Kunugi, A. Canavesi, S. Rigaut, C. N. Moorefield and G. R. Newkome, *Chem. Mater.*, 1998, **10**, 1751–1754.
10 S. Deng, J. Locklin, D. Patton, A. Baba and R. C. Advincula, *J. Am. Chem. Soc.*, 2005, **127**, 1744–1751.
11 C. Xia, X. Fan, J. Locklin and R. C. Advincula, *Org. Lett.*, 2002, **4**, 2067–2070.
12 N. Negishi, Y. Ie, M. Taniguchi, T. Kawai, H. Tada, T. Kaneda and Y. Aso, *Org. Lett.*, 2007, **9**, 829–832.
13 Y. Zhang, C. Zhao, J. Yang, M. Kapiamba, O. Haze, L. J. Rothberg and M. K. Ng, *J. Org. Chem.*, 2006, **71**, 9475–9483.
14 Y. Geng, A. Fechtenkötter and K. Müllen, *J. Mater. Chem.*, 2001, **11**, 1634–1641.
15 A. Bilge, A. Zen, M. Forster, H. Li, F. Galbrecht, B. S. Nehls, T. Farrell, D. Neher and U. Scherf, *J. Mater. Chem.*, 2006, **16**, 3177–3182.
16 X. B. Sun, Y. Q. Liu, S. Y. Chen, W. F. Qiu, G. Yu, Y. Q. Ma, T. Qi, H. J. Zhang, X. J. Xu and D. B. Zhu, *Adv. Funct. Mater.*, 2006, **16**, 917–925.
17 T. M. Pappenfus and K. R. Mann, *Org. Lett.*, 2002, **4**, 3043–3046.
18 J. Pei, J. L. Wang, X. Y. Cao, X. H. Zhou and W. B. Zhang, *J. Am. Chem. Soc.*, 2003, **125**, 9944–9945.
19 C.-C. You, C. R. Saha-Möller and F. Würthner, *Chem. Commun.*, 2004, 2030–2031.
20 Y. Nicolas, P. Blanchard, E. Levillain, M. Allain, N. Mercier and J. Roncali, *Org. Lett.*, 2004, **6**, 273–276.
21 S. Roquet, R. de Bettignies, P. Leriche, A. Cravino and J. Roncali, *J. Mater. Chem.*, 2006, **16**, 3040–3045.
22 X.-M. Liu, C. He and J. Huang, *Tetrahedron Lett.*, 2004, **45**, 6173–6177.
23 S. A. Ponomarenko, E. A. Tatarinova, A. M. Muzafarov, S. Kirchmeyer, L. Brassat, A. Mourran, M. Moeller, S. Setayesh and D. deLeeuw, *Chem. Mater.*, 2006, **18**, 4101–4108.
24 C.-Q. Ma, E. Mena-Osteritz, T. Debaerdemaeker, M. M. Wienk, R. A. J. Janssen and P. Bäuerle, *Angew. Chem. Int. Ed.*, 2007, **46**, 1679–1683.
25 C.-Q. Ma, M. Fonrodona, M. C. Schikora, M. M. Wienk, R. A. J. Janssen and P. Bäuerle, *Adv. Funct. Mater.*, 2008, **18**, 3323–3331.
26 M. K. R. Fischer, T. E. Kaiser, F. Würthner and P. Bäuerle, *J. Mater. Chem.*, 2009, **19**, 1129–1141.
27 W. M. Albers, G. W. Canters and J. Reedijk, *Tetrahedron*, 1995, **51**, 3895–3904.
28 R. Nakajima, H. Iida and T. Hara, *Bull. Chem. Soc. Jpn.*, 1990, **63**, 636–637.
29 E. C. Constable, C. E. Housecroft, M. Neuburger and C. X. Schmitt, *Polyhedron*, 2006, **25**, 1844–1863.
30 H. F. Lu, H. S. O. Chan and S. C. Ng, *Macromolecules*, 2003, **36**, 1543–1552.
31 L. Trouillet, A. De Nicola and S. Guillerez, *Chem. Mater.*, 2000, **12**, 1611–1621.
32 F. Lafolet, F. Genoud, B. Divisia-Blohorn, C. Aronica and S. Guillerez, *J. Phys. Chem. B*, 2005, **109**, 12755–12761.
33 K. A. Walters, L. Trouillet, S. Guillerez and K. S. Schanze, *Inorg. Chem.*, 2000, **39**, 5496–5509.
34 Y. Li, K. Kamata, S. Asaoka, Y. T. and T. Iyoda, *Org. Biomol. Chem.*, 2003, **1**, 1779–1784.
35 F. Steybe, F. Effenberger, U. Gubler, C. Bosshard and P. Gunter, *Tetrahedron*, 1998, **54**, 8469–8480.
36 A. Abbotto, S. Bradamante, A. Facchetti and G. A. Pagani, *J. Org. Chem.*, 1997, **62**, 5755–5765.
37 C.-Q. Ma, M. K. R. Fischer and P. Bäuerle, *Chem. Asian J.*, 2008, submitted.
38 T. C. Chou, C. L. Hwa, J. J. Lin, K. C. Liao and J. C. Tseng, *J. Org. Chem.*, 2005, **70**, 9717–9726.
39 A. Bacchi, E. Bosetti, M. Carcelli, P. Pelagatti and D. Rogolino, *Eur. J. Inorg. Chem.*, 2004, 1985–1991.
40 M. Mardelli and J. Olmsted, *J. Photochem.*, 1977, **7**, 277–285.
41 M. M. Martin, *Chem. Phys. Lett.*, 1975, **35**, 105–111.
42 J. Catalan, E. Mena, W. Meutermans and J. Elguero, *J. Phys. Chem.*, 1992, **96**, 3615–3621.
43 R. W. Taft, J.-L. M. Abboud and M. J. Kamlet, *J. Am. Chem. Soc.*, 1981, **103**, 1080–1086.
44 N. R. Adams, *Electrochemistry at Solid Electrodes*, M. Dekker: New York, 1969.
45 T. Johansson, W. Mammo, M. Svensson, M. R. Andersson and O. Inganas, *J. Mater. Chem.*, 2003, **13**, 1316–1323.

46 B. C. Thompson and J. M. J. Fréchet, *Angew. Chem. Int. Ed.*, 2008, **47**, 58–77.
47 Y. Zhou, P. Peng, L. Han and W. Tian, *Synth. Met.*, 2007, **157**, 502–507.
48 S. Roquet, A. Cravino, P. Leriche, O. Alévêque, P. Frere and J. Roncali, *J. Am. Chem. Soc.*, 2006, **128**, 3459–3466.
49 A. Cravino, P. Leriche, O. Alévêque, S. Roquet and J. Roncali, *Adv. Mater.*, 2006, **18**, 3033–3037.
50 K. Takahashi, N. Kuraya, T. Yamaguchi, T. Komura and K. Murata, *Sol. Energy Mater. Sol. Cells*, 2000, **61**, 403–416.
51 F. A. Castro, A. Faes, T. Geiger, C. F. O. Graeff, M. Nagel, F. Nuesch and R. Hany, *Synth. Met.*, 2006, **156**, 973–978.
52 F. Meng, K. Chen, H. Tian, L. Zuppiroli and F. Nuesch, *Appl. Phys. Lett.*, 2003, **82**, 3788–3790.
53 M. Jørgensen and F. C. Krebs, *J. Org. Chem.*, 2004, **69**, 6688–6696.